# MAS-DNP Enhancements: Hyperpolarization, Depolarization, and Absolute Sensitivity

Sabine Hediger, Daniel Lee, Frederic Mentink-Vigier, Gaël de Paëpe

# MAS-DNP Enhancements: Hyperpolarization, Depolarization, and Absolute Sensitivity

Sabine Hediger[1,2], Daniel Lee[1], Frédéric Mentink-Vigier[3], and Gaël De Paëpe[1]

[1]*Univ. Grenoble Alpes, CEA,* [2]*CNRS, INAC-MEM, F-38000 Grenoble, France.*

[3]*CIMAR-National High Magnetic Field Laboratory, Tallahassee, FL 32310 USA.*

## 1. Introduction

Since the earliest days of solid-state Dynamic Nuclear Polarization (DNP) and the first experiment by Carver and Slichter on lithium,[1] the ability of this technique to enhance the polarization of nuclear spins has been quantified by comparing the NMR signal obtained under suitable microwave (μwave) irradiation of the electron spins with the same signal in absence of this irradiation. This is a very direct and easy experiment which immediately reflects the gain in sensitivity obtained on the NMR experiment by making use of the larger electron spin polarization. This DNP enhancement factor, normally denoted $\varepsilon$ with various indices (depending on the polarization transfer mechanism, on the targeted isotope, on the permanently on-going developments, etc.) has accompanied all the instrumental and technical developments that have been required to make DNP compatible with experimental conditions of modern high-resolution high-field solid-state NMR.[2–4] Whereas the step-wise evolution to higher magnetic fields impacted each time negatively on the enhancement, as expected from the inverse field dependence of the ubiquitous DNP mechanisms, the enhancement factor, called in this contribution $\varepsilon_{on/off}$, was able to recover somewhat through improvements to the source of electron spins, known as the polarizing agent (PA). A first move from BDPA and the solid-effect (SE) mechanism[5] to nitroxide radicals in frozen aqueous solutions using the cross effect (CE)[6] led to the introduction of bis-nitroxide PAs[7] and a water soluble version TOTAPOL.[8] With the arrival of the first commercial DNP spectrometer at 9.4 T in 2010,[9] a growing number of research groups have become involved in these modern DNP developments, and values of $\varepsilon_{on/off}$ have increased regularly with the introduction of new bis-nitroxide radicals or modifications of existing ones,[10–17] designed to improve the DNP efficiency and/or to broaden the applicability of the technique by modifying solubility conditions. At the time of this writing, the "gold standards" in magic angle spinning (MAS) DNP under the most common conditions of 9.4 T and 100 K are AMUPol[15] for aqueous frozen solutions and TEKPol[14] for organic

solvents, both leading to proton enhancement factors of more than 200 in optimal samples.[16,17] Considering that the theoretical limit for the enhancement of protons via DNP under continuous μwave irradiation is 658, given by the ratio between electron and proton gyromagnetic ratios, these recent experimental results suggest that about 1/3 of the electron polarization could effectively be transferred to the surrounding proton spins.

Going further in the optimization of the DNP process itself, it was shown that the incorporation of dielectric solid particles and removal of dissolved paramagnetic oxygen through degassing of the frozen solution amplifies the DNP enhancement by improving μwave propagation and increasing spin relaxation times, respectively, and $\varepsilon_{on/off}$ of 515 has been observed.[18] Lowering the sample temperature is also known to slow down the relaxation of both the electron and nuclear spins thus improving the transfer of polarization. In this context a DNP enhancement factor of 677, astonishingly above the "theoretical limit" of 658, has been reported for MAS-DNP using AMUPol for the CE at a sample temperature of 55 K.[19] This required using a closed-loop recirculating helium system for spinning and cooling.[19,20]

These latter enhancement factors of course look very promising at first sight, but they require a critical review. Considering the CE mechanism, which is now the most established for current standard MAS-DNP conditions and used in the aforementioned studies, the theoretical maximum value of 658 could only then be achieved, if one electron spin of the biradical can be completely saturated by the continuous μwave irradiation, without impacting the second electron at all, and the difference of polarization between the two electron spins can entirely be transferred to proton spins. Under MAS, both steps happen successively in so-called rotor events (see next section)[21–23] corresponding to crossing or anti-crossing of some of the energy levels of the 3-spin system, which are modulated through the MAS. The μwave field strength for electron irradiation has been reported to be < 1 MHz for an input power of 5 W at

high magnetic field,[24,25] a realistic value for the actual instrumentation. It is of the same order of magnitude as the inverse of the phase memory times $T_m$[a] (or $T_{2e}$) reported for bis-nitroxide radicals used in MAS-DNP conditions (around 0.6-4 μs).[14,16,17] However, even if the μwave irradiation is performed in a continuous-wave modus, attempted saturation of single electron spins happens via the short rotor events that are periodically repeated according to the MAS frequency. As such, this saturation process is in competition with the longitudinal electron relaxation $T_{1e}$, which is on the order of the rotor period for bis-nitroxides at the temperature and spinning frequencies standardly used for MAS-DNP (about 100 K and 5-40 kHz).[14,16] Under such conditions, and even without considering the losses through other non-ideal types of rotor events, it is then questionable that full saturation of one electron spin can occur and a hyperpolarization close to 80-100%, as suggested by the above reported record $\varepsilon_{on/off}$ enhancement factors, can experimentally be obtained with hyperpolarization agents known so far.[b] It is therefore crucial to understand the origin of the potential discrepancy between $\varepsilon_{on/off}$ and the real polarization obtained in a MAS-DNP experiment. This will be the focus of the next section.

Another perturbing aspect of the enhancement ratio $\varepsilon_{on/off}$ consists in its lack of information about the actual NMR sensitivity from a DNP experiment. This is nicely illustrated in the simple example on glycine by Takahashi *et al.*, which is reproduced in Figure 1.[26] Whereas an encouraging $\varepsilon_{on/off}$ of 20 was obtained using TOTAPOL for a frozen solution of 0.1 M [2-$^{13}$C]-glycine, one of the standard ways to prepare a DNP sample, the sensitivity of the MAS-DNP enhanced signal, defined as the signal-to-noise ratio per unit square root of the

[a] In EPR, the phase memory time $T_m$ is the characteristic time describing the decay of the electron-spin Hahn-echo intensity with increasing echo time. It corresponds to the refocused transverse relaxation time in solid-state NMR, denoted $T_2$'. For homogeneously broadened EPR spectra, $T_m$ corresponds to the transverse relaxation time $T_{2e}$.
[b] In dissolution DNP, 91% of polarization on $^1$H can be achieved at the more favorable conditions of 1.2 K and 6.7 T. The build-up time for the hyperpolarization is however 150 s.[66]

experimental time, $(S/N)_{\sqrt{t}}$, was almost 50× less than the sensitivity obtained with standard solid-state MAS-NMR on a powdered sample. A high $\varepsilon_{on/off}$ value may therefore be informative on a well-working hyperpolarization mechanism, but cannot be used alone to estimate the gain in sensitivity and experimental time one can obtain by using MAS-DNP. Several groups have addressed this problem of quantifying correctly the sensitivity enhancement of MAS-DNP experiments, and a survey of the different solutions proposed will be presented.

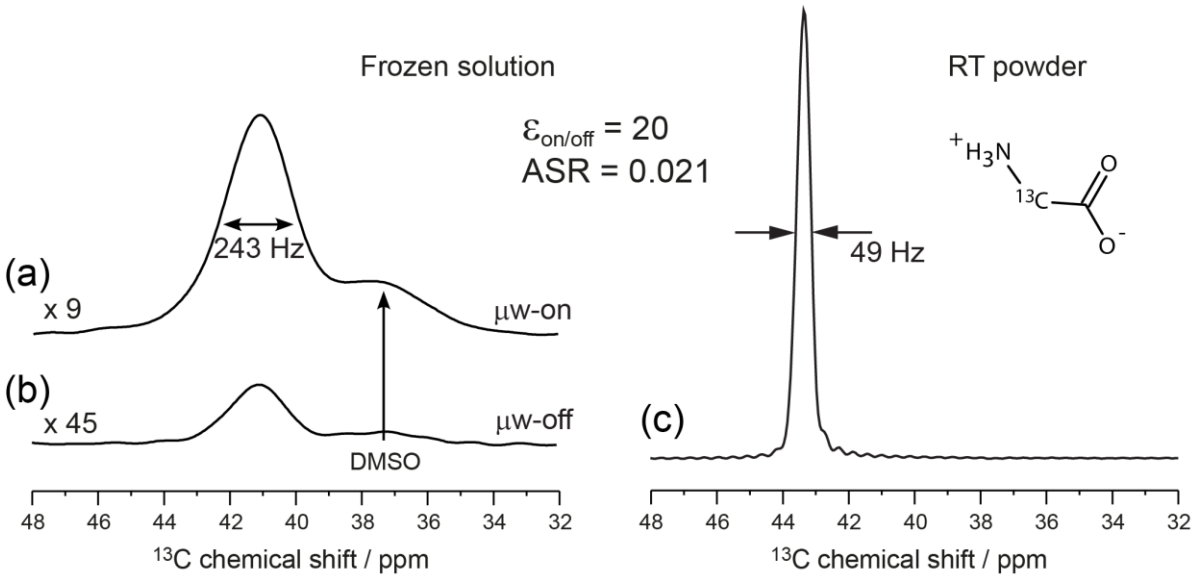


***Figure 1.*** *$^{13}$C CPMAS spectra of [2-$^{13}$C]-glycine recorded at 9.4 T using a MAS frequency of 8 kHz. (a)-(b) Frozen solution of 0.1 M [2-$^{13}$C]-glycine in $d_6$-DMSO/$D_2O$/$H_2O$ (6:3:1 v/v/v) with 20 mM TOTAPOL, recorded at 105 K with (a) and without (b) μwave irradiation for CE DNP. (c) Powder sample of [2-$^{13}$C]-glycine recorded at RT using conventional solid-state NMR. ASR (Absolute Sensitivity Ratio) is the ratio of $(S/N)_{\sqrt{t}}$ between the spectra obtained under DNP and standard ssNMR conditions. Adapted with permission from Ref. [26] Copyright 2012 Wiley-VCH Verlag GmbH &Co. KGaA, Weinheim.*

In the jungle of different ways that have been proposed to measure the efficiency of MAS-DNP to enhance NMR spectra, the DNP investigator has good reasons to be lost, not knowing which factor would be the most relevant to assert one's findings in terms of DNP sensitivity. We will therefore in the conclusion section go through different types of DNP studies and developments to highlight the corresponding relevant measure of the DNP-enhanced NMR sensitivity.

## 2. The force of $\varepsilon_{on/off}$ and its dark side

To better understand the dark side of $\varepsilon_{on/off}$ without going into the deepest details of the CE theory under MAS, we will first consider a simplified thermodynamical picture of the CE mechanism under static conditions, which will then be extended to MAS. Thorough theoretical descriptions of the CE at high magnetic field in static[3,27] and under MAS[21,22] conditions, inclusive of depolarization,[28,29] can be found elsewhere.[30]

### 2.1 CE DNP in static samples

Hyperpolarization by CE happens in a 3-spin system composed of two coupled electron spins, with respective EPR transition frequencies $\omega_{e1}$ and $\omega_{e2}$, and one coupled nuclear spin with Larmor frequency $\omega_n$. The CE condition requires the difference between the two electron-spin frequencies to match the nuclear Larmor frequency, $\omega_{e1} - \omega_{e2} = \pm\omega_n$ (see Figure 2a). This condition can be experimentally observed for PAs whose EPR transition is inhomogeneoulsy broadened by the *g*-anisotropy such that the frequency range of the EPR line is larger than the Larmor frequency of the considered nuclear spin (see Figure 2a). Coupled electron spins whose respective *g*-tensor orientations are such that the CE condition is met can then produce hyperpolarization of the nuclear spin when μwave irradiation is applied to the EPR transition of one of the two electron spins.

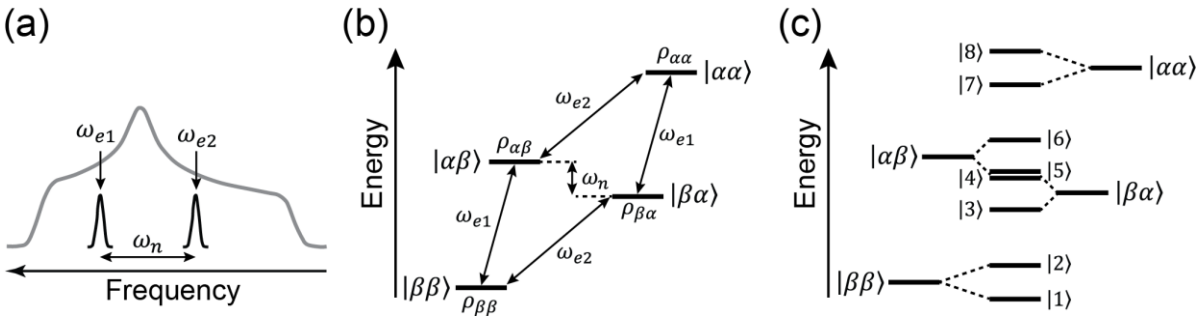


***Figure 2.*** *(a) Schematic representation of the EPR line of a nitroxide radical, inhomogeneoulsy broadened by the g-anisotropy, with the selection of two crystallite orientations whose respective EPR*

*frequencies $\omega_{e1}$ and $\omega_{e2}$ are separated by the Larmor frequency of the nuclear spin $\omega_n$. (b) Energy level diagram for the two coupled electron spins of (a). The change in energy due to the dipolar coupling is neglected. The energy levels are labeled according to the spin state $\alpha$ or $\beta$ of each electron. (c) Energy level diagram for a 3-spin system composed of the two previous electron spins coupled to one nuclear spin. The energy levels are numbered from* $|1\rangle$ *to* $|8\rangle$.

Let us consider an arbitrary irradiation at the frequency of $\omega_{e1}$ (the same reasoning can be done at $\omega_{e2}$). The populations of the four energy levels of the two-electron spin system (see Figure 2b), originally at their Boltzmann equilibrium (denoted $\rho_{ij}^{\mathrm{eq}}$ with $i,j = \beta\ or\ \alpha$, the two spin–1/2 states), will be perturbed such to approach population equilibration of the energy levels corresponding to the spin transition of the 1st electron:

$$\begin{aligned} \rho_{\alpha\beta} &= \tfrac{1}{2}\left[(2-s)\rho_{\alpha\beta}^{\mathrm{eq}} + s\rho_{\beta\beta}^{\mathrm{eq}}\right] \quad \rho_{\alpha\alpha} = \tfrac{1}{2}\left[(2-s)\rho_{\alpha\alpha}^{\mathrm{eq}} + s\rho_{\beta\alpha}^{\mathrm{eq}}\right] \\ \rho_{\beta\beta} &= \tfrac{1}{2}\left[(2-s)\rho_{\beta\beta}^{\mathrm{eq}} + s\rho_{\alpha\beta}^{\mathrm{eq}}\right] \quad \rho_{\beta\alpha} = \tfrac{1}{2}\left[(2-s)\rho_{\beta\alpha}^{\mathrm{eq}} + s\rho_{\alpha\alpha}^{\mathrm{eq}}\right] \end{aligned} \qquad (1)$$

with *s*, the saturation factor, which takes values between 0 in absence of irradiation and 1 for irradiation able to completely saturate the $\omega_{e1}$ transition. The polarization $P_{e1}$ and $P_{e2}$ for the two electron spins, obtained from the energy-levels' population difference is then:

$$\begin{aligned} P_{e1} &= (1-s)P_{e1}^{\mathrm{eq}} \\ P_{e2} &= P_{e2}^{\mathrm{eq}} \end{aligned} \qquad (2)$$

with $P_{e1}^{\mathrm{eq}}, P_{e2}^{\mathrm{eq}}$ the thermal equilibrium Boltzmann polarizations of the two electron spins. Due to the (partial) saturation of the 1st electron spin under μwave irradiation, its polarization is reduced towards 0 depending on the saturation factor, whereas the polarization of the 2nd electron is maintained at its thermal equilibrium. If we now consider that the 2-electron spins system is coupled to a nuclear spin, each of the four electron energy levels is split into two levels separated by an energy corresponding to $\omega_n$ (Figure 2c). Their respective populations $\rho_{ij}$ are spread on the two levels with a difference corresponding to the thermal equilibrium

nuclear polarization $P_n^{\mathrm{eq}}$. When the CE condition is met, levels $|4\rangle$ and $|5\rangle$, with respective populations of $\rho_4 = \rho_{\beta\alpha} - \frac{P_n^{\mathrm{eq}}}{2}$ and $\rho_5 = \rho_{\alpha\beta} + \frac{P_n^{\mathrm{eq}}}{2}$ to first approximation, are degenerate, leading to strong state mixing with the mixed eigenstates $|4\rangle_m = \frac{1}{\sqrt{2}}(|4\rangle + |5\rangle)$ and $|5\rangle_m = \frac{1}{\sqrt{2}}(|4\rangle - |5\rangle)$. The coupling element between these two levels (composed of the dipolar and hyperfine couplings) will lead to an equilibration of the populations and the mixed states will end up with the populations

$$\rho_4^{\mathrm{mixed}} = \rho_5^{\mathrm{mixed}} = \frac{1}{2}\left(\rho_{\alpha\beta} + \rho_{\beta\alpha}\right). \qquad (3)$$

The nuclear spin polarization obtained from the population difference between levels $|3\rangle$ and $|4\rangle_m$ as well as $|5\rangle_m$ and $|6\rangle$ is then (provided that two-spin or three-spin order are not created)

$$P_n^{\mathrm{on}} = \frac{1}{2}\left(P_{e1} - P_{e2} + P_n^{\mathrm{eq}}\right) = \frac{1}{2}\left(\Delta P_e + P_n^{\mathrm{eq}}\right), \qquad (4)$$

with $P_{e1}$ and $P_{e2}$ given in Eq. (2). At the CE condition, we can consider that the nuclear polarization is put into contact with the electron polarization difference created by the μwave irradiation. Of course, we have to keep in mind that the electron transition $\omega_{e1}$ (or $\omega_{e2}$) is continuously irradiated during the whole process. This maintains the electron polarization difference $\Delta P_e$ at the same level despite continuous transfer of polarization to the nuclear spin. $P_n^{\mathrm{on}}$ increases therefore above the value given in Eq. (4) until it reaches, in the limit of infinite nuclear longitudinal relaxation $T_{1n}$, the same value as the electron polarization difference (quasi-equilibrium state),

$$P_n^{\mathrm{on}} \to \Delta P_e. \qquad (5)$$

The nuclear spin hyperpolarization is transferred to distant coupled nuclear spins via spin-diffusion.[31,32] This process is however not described further here. In absence of irradiation

($s = 0$), the reasoning leading to Eq. (5) still applies as long as the CE condition is met. In this case, the difference in polarization of the two electron spins $\Delta P_e$ corresponds to the Boltzmann polarization difference, which is proportional to the difference in frequencies of the two electrons, $\Delta P_e(s = 0) \propto (\omega_{e1} - \omega_{e2})$, and therefore equal to the nuclear Boltzmann polarization (as expected for the CE condition). The nuclear polarization is thus not modified and

$$P_n^{\text{off}} = \Delta P_e^{\text{eq}} = P_n^{\text{eq}} \tag{6}$$

This apparent trivial result will highlight its importance once MAS is introduced.

In the case of a substantial irradiation, $s > 0$, the difference in electron polarization $\Delta P_e$ is negative for irradiation at $\omega_{e1}$ and positive for irradiation at $\omega_{e2}$, corresponding to negative and positive enhancement of the nuclear polarization, respectively. In the optimum case of complete saturation, $s = 1$, the nuclear spin polarization will be enhanced up to the electron polarization, $P_n^{\text{on}}(s = 1) = P_e^{\text{eq}}$, leading to the already mentioned upper limit for the enhancement factor:

$$\max\left(\varepsilon_{\text{on/off}}^{\text{static}}\right) = \frac{P_n^{\text{on}}(s=1)}{P_n^{\text{off}}} = \frac{P_e^{\text{eq}}}{P_n^{\text{eq}}} = \frac{\gamma_e}{\gamma_n}. \tag{7}$$

For protons ($n$ = $^1$H), this ratio is 658.[c] In practice, several factors prevent obtaining the maximal value: obviously an incomplete saturation factor (depends on the μwave power and the homogeneous linewidth, and therefore on $T_m$), but also the longitudinal electron and nuclear relaxation times $T_{1e}$ and $T_{1n}$, which continuously fight against the out-of-equilibrium situation encountered under μwave irradiation.

[c] In the situation where the polarization of one electron spin could be inverted, instead of saturated, the theoretical maximum enhancement would be 1316. This would require coherent control on the electron spins by i.e. pulsed DNP.[67]

### 2.2. CE DNP in Magic Angle Spinning samples

Under MAS, the frequencies $\omega_{e1}$ and $\omega_{e2}$ of the two coupled electron spins (see Fig. 2a) are not fixed any more, but move across the EPR line, due to the relative reorientation of the respective *g*-tensors of the electron spins. As a result, the 8 energy levels of the 2-electrons-1-nucleus spin system are modulated with the MAS frequency $\omega_r$, as can be seen in Figure 3a.

During the course of the rotor period, the different energy levels can occasionally and sequentially fulfill some different conditions, called rotor events.[21,22] It is the periodic succession of these discrete rotor events that bring the spin system to a quasi-periodic out-of-equilibrium state. There are four types of rotor events: (i) μwave rotor events, when the resonant frequency of one electron spin matches the μwave frequency, $\omega_{e,i} = \omega_{\mu w}$ (*i*=1, 2); (ii) CE rotor events, when the electron frequencies match the CE condition $|\omega_{e1} - \omega_{e2}| = \omega_n$; (iii) dipolar events, when the two electron spin frequencies are identical $\omega_{e1} = \omega_{e2}$; (iv) solid-effect (SE) events when the SE condition is met $|\omega_{e,i} - \omega_{\mu w}| \approx \omega_n$ (see Figure 3).

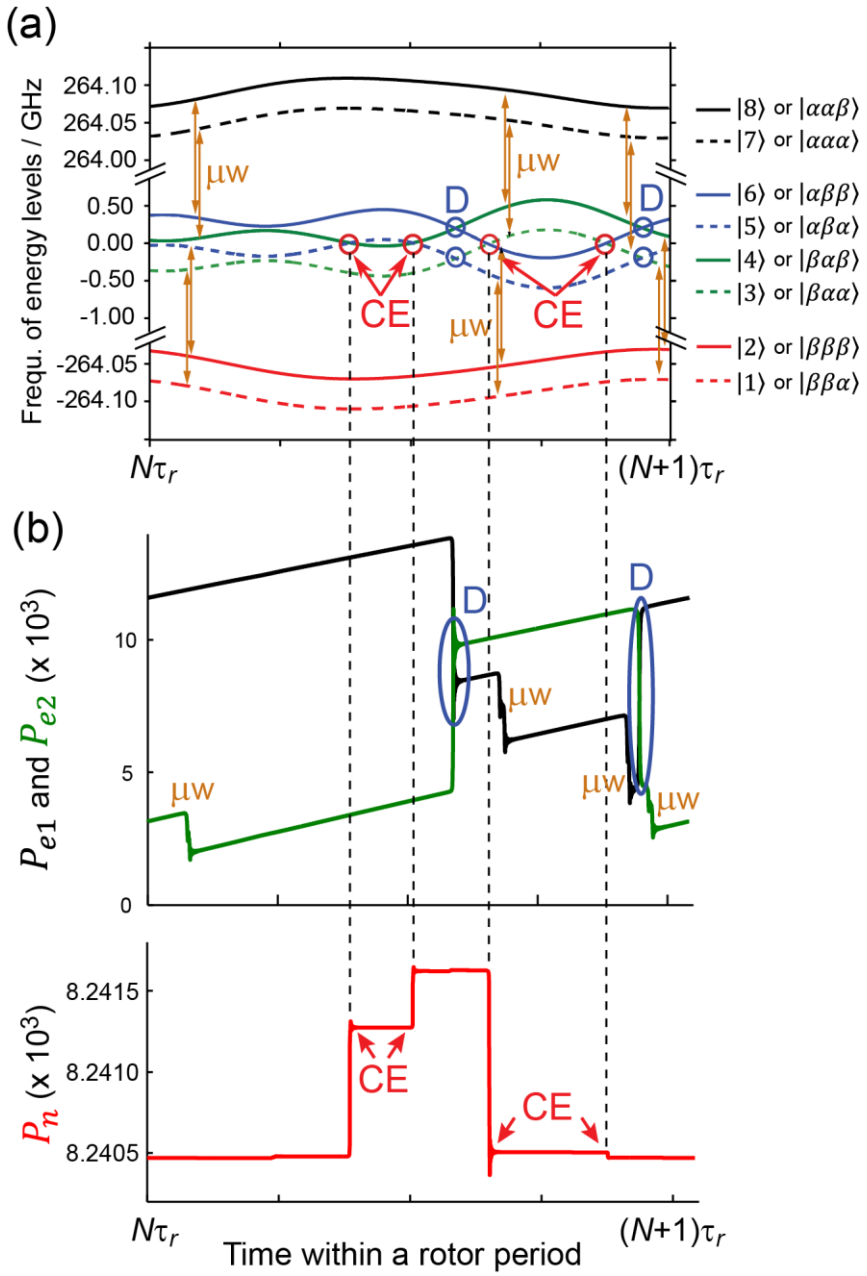


***Figure 3.*** *(a) Time evolution during a steady-state rotor period of the frequencies of the 8 energy levels of Fig. 2c under MAS for one crystallite. μwave rotor events (μw) are indicated by orange vertical arrows, CE and dipolar (D) rotor events by red and blue circles, respectively. Color and line code for the different levels is given next to the figure. (b) Corresponding evolution of the polarization for the 1st electron spin in black, for the 2nd electron spin in green, and for the nuclear spin in red.*

Rotor events (i) and (ii) are essential to obtain CE hyperpolarization under MAS, and they act exactly the same as in the static thermodynamical picture given above, except that their effect is (normally) sequential. Each time the modulated energy levels experience a μwave rotor event, the polarization of the corresponding electron spin will be decreased by a partial

saturation. This modifies the difference in electron polarization, $\Delta P_e$, which later will partially exchange with the nuclear polarization $P_n$ whenever a CE rotor event is encountered. The dipolar coupling (besides the *J* exchange interaction) between the two electrons leads to an exchange of polarization between the two electrons during the so-called dipolar rotor events (iii). The SE rotor events (iv) will be neglected here as their effect is marginal under conditions chosen to optimize CE for protons using nitroxide-based PAs. The transfer efficiency of all rotor events depends on the effective strength of the active interaction, as well as on the relaxation times and spinning frequency, which all together define the degree of adiabaticity for the fast passage crossings or anticrossings. Thus, dipolar events will entirely exchange polarization, and therefore keep the already built difference in electron polarization, $|\Delta P_e|$, only if the effective dipolar (or *J* exchange) coupling element is strong enough. If the coupling element is too small, the polarization exchange will be incomplete resulting in a reduction of $|\Delta P_e|$. This is for example one reason hyperpolarization gets less efficient when the biradical concentration is too high and the intermolecular dipolar coupling to a third electron spin can no longer be neglected.[29,33]

The buildup of nuclear polarization under MAS is therefore complex and requires proper computational tools to obtain the result of the successive different rotor events for all orientations encountered in a solid sample.[23,33] We now focus on two aspects that have been shown to be relevant for sensitivity considerations: the electron and nuclear spin polarizations in absence of μwave irradiation and the buildup time of nuclear hyperpolarization.

**Electron and nuclear spin polarization in absence of μwave irradiation.** In absence of μwave irradiation, which is the situation encountered when the "off" signal is measured, the energy levels of the spin system are modulated exactly the same way as under irradiation, and all rotor events are active except the μwave rotor events. For instance, at each CE rotor event,

the nuclear polarization will still equilibrate with the difference of electron spin polarization. However, under MAS, the thermal electron spin polarizations are (partially) averaged by the MAS rotation towards values proportional to the isotropic frequency of their respective *g*-tensors. For nitroxides and bis-nitroxides, the two coupled electron spins can therefore have very similar polarization under MAS. In absence of irradiation, the difference of polarization $|\Delta P_e|$ can therefore become very small and even tend towards 0 when the $T_{1e}$ gets much longer than the rotor period. In such a case, the Boltzmann nuclear polarization can be larger than the difference of electron polarization, and each CE rotor event will lead to a decrease of nuclear polarization to compensate for the smaller difference of electron polarization, until a new quasi-equilibrium is reached, below the nuclear Boltzmann thermal equilibrium. Therefore under MAS, the "off" signal reflects a depolarized nuclear state compared to the thermal value measured for static conditions, $P_n^{\text{off, MAS}} = \varepsilon_{\text{depo}} \cdot P_n^{\text{eq}}$, with $\varepsilon_{\text{depo}}$ (also called $\chi_{\text{Depo}}$ in ref. [34]) taking values between 0 and 1 for protons with the biradicals investigated so far. As soon as irradiation is turned "on", a large difference of electron polarization will be created, allowing for hyperpolarization of the nuclear spins. The traditional $\varepsilon_{\text{on/off}}$ measured as the ratio between the NMR signal intensity with and without μwave irradiation needs therefore to be corrected under MAS by the depolarization factor $\varepsilon_{\text{depo}}$ to reflect the real polarization gain with respect to Boltzmann equilibrium, $\varepsilon_B = \varepsilon_{\text{on/off}} \cdot \varepsilon_{\text{depo}}$.

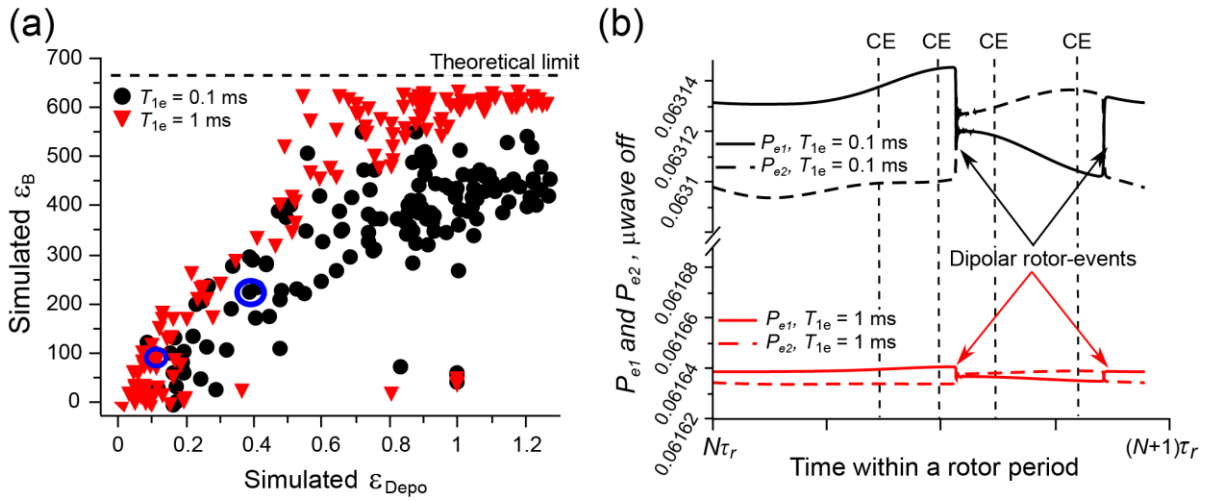


***Figure 4.*** *(a) Correlation of the simulated $^1$H hyperpolarization obtained in presence of μwave irradiation and normalized by Boltzmann thermal equilibrium (simulated $\varepsilon_B$), with the simulated $^1$H depolarization observed in absence of irradiation (simulated $\varepsilon_{depo}$) for 144 different crystallite orientations of a bis-nitroxide, considering two different electron spin relaxation time constants $T_{1e}$ of 0.1 ms (in black) and 1 ms (in red) and a MAS frequency set at 12.5 kHz. (b) Simulation of the electron polarization $P_{e1}$ and $P_{e2}$ (full and dashed lines) over one rotor period $\tau_r$ after $N\tau_r$ = 8.33 s of evolution without μwave irradiation (quasi-equilibrium reached) for the crystal orientation circled in blue in (a), using the same color code as in (a). Adapted from Ref. [29] with permission from the PCCP Owner Societies.*

As shown in ref. [29], nuclear spin depolarization increases for longer $T_{1e}$, as the averaging of the *g*-tensor by MAS is then more efficient, and in addition the recovery of polarization difference after an inefficient dipolar rotor event will be minor (see Figure 4b). It explains, at least in part, why AMUPol is found to depolarize more than TOTAPOL.[29] It is important to realize that it is the same CE mechanism that leads to nuclear depolarization in absence of irradiation as for nuclear hyperpolarization when irradiation is turned on. It is therefore not astonishing that there is a correlation between the capacity of bis-nitroxide orientations to depolarize and hyperpolarize, as shown in the simulations of Figure 4a. The enhancement ratio $\varepsilon_{on/off}$ under MAS reflects therefore not only the ability of a biradical to hyperpolarize, but the sum of its depolarization and hyperpolarization capacities, with respect to the Boltzmann equilibrium, as sketched in Figure 5. This renders the quantitative comparison

of biradicals for CE DNP on the basis of their $\varepsilon_{on/off}$ alone seriously flawed. The introduction in 2013 of the rigid biradical AMUPol[15] provided a huge jump in $\varepsilon_{on/off}$ of a factor of more than 4 (up to 6 at 10 kHz MAS frequency) compared to TOTAPOL.[29] However, in reality, a longer $T_{1e}$ resulting from a more rigid biradical can enhance depolarization even more than hyperpolarization, and, for AMUPol, the real gain with respect to Boltzmann equilibrium is only up to 3 at 10 kHz MAS frequency and 110 K.[29] Until recently, all studies to improve the efficiency of biradicals were based on $\varepsilon_{on/off}$, and we can therefore expect that some PAs may have been wrongly rejected.

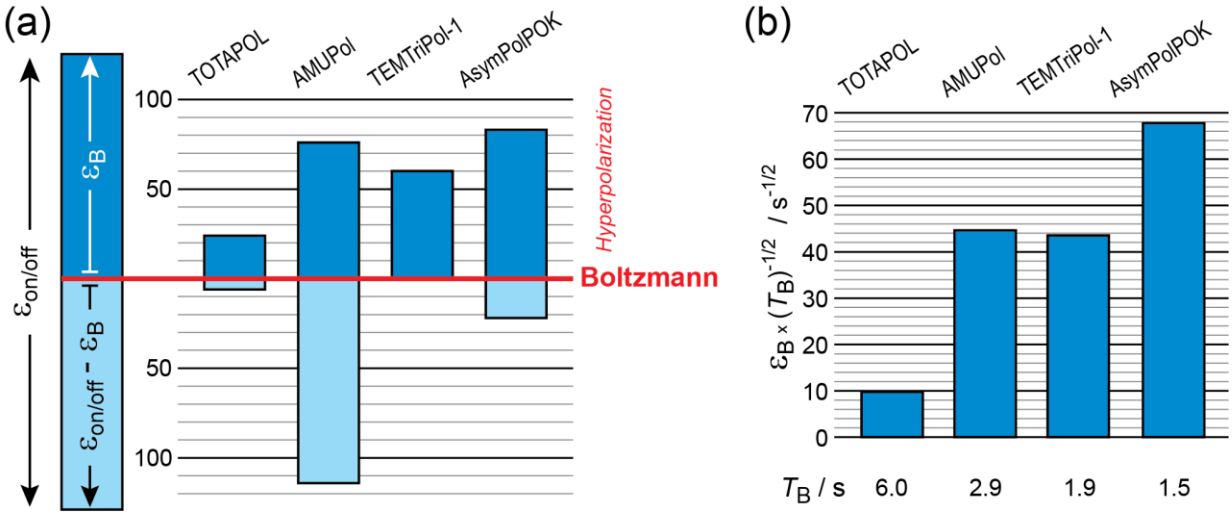


***Figure 5.*** *(a) Schematic representation of the Boltzmann hyperpolarization contribution (dark blue) to experimental* $\varepsilon_{on/off}$ *at 9.4 T,10 kHz MAS frequency, and 110 K for different water soluble biradicals: TOTAPOL, AMUPol, TEMTriPol-1 and AsymPolPOK. Note that the size of the light blue bars only represents the discrepancy between* $\varepsilon_{on/off}$ *and* $\varepsilon_B$*. It is not proportional to the amount of depolarization, which cannot be larger than the nuclear Boltzmann polarization,* $P_n^{eq} - P_n^{off,\,MAS} = (1 - \varepsilon_{depo})P_n^{eq}$*. Experimental values for* $\varepsilon_{on/off}$ *and* $\varepsilon_B$ *(the enhancement ratio with respect to Boltzmann equilibrium) are taken from Ref. [29] for TOTAPOL and AMUPol, Ref.* [34] *for TEMTriPol-1 and Ref.* [35] *for AsymPolPOK. The biradical concentration was 12 mM for TOTAPOL and AMUPol, and 10 mM for TEMTriPol-1 and AsymPolPOK, in a standard DNP glassy matrix. Other experimental details can be found in the corresponding references. (b) Schematic representation of the sensitivity, expressed as the enhancement factor* $\varepsilon_B$ *divided by the square root of the hyperpolarization build-up time constant* $T_B$*, for the same biradicals as in (a). Experimental values for* $T_B$ *are given below each bar and are taken from the same references as data for (a).*

Two recent studies have highlighted that efficient biradicals for CE under MAS, which present reduced and even no depolarization, are possible. TEMtriPol-1[36] is a TEMPO-trityl-based mixed biradical. The different nature of the two coupled electron spins is such that their isotropic frequencies differ by about the proton nuclear Larmor frequency. Thanks to this particular spectral signature, the MAS-averaged difference of electron spin polarization in absence of irradiation matches approximatively the $^1$H Boltzmann equilibrium nuclear spin polarization, thus avoiding depolarization.[d] Despite a much smaller $\varepsilon_{on/off}$, the enhancement ratio with respect to Boltzmann thermal equilibrium, $\varepsilon_B$, is only slightly less than for AMUPol at 9.4 T. The main advantage of TEMTriPol-1 is at higher fields where it becomes much more efficient than AMUPol (4 times more at 18.8 T[34]). AsymPolPOK[35] is an asymmetric biradical as well, which links together 5-membered and 6-membered ring nitroxides. It is the first biradical that has been specifically designed to optimize $\varepsilon_B$, and not $\varepsilon_{on/off}$. This was achieved by combining these rings by a short, electron rich linker, resulting in an increased dipolar electron interaction and a large *J* exchange interaction. These strong electron-electron interactions promote efficient hyperpolarization while keeping a reduced depolarization.

**Buildup time of hyperpolarized nuclear polarization.** Except for the special case of single-scan spectroscopy, modern Fourier-transform NMR relies on signal averaging of several transients. The sensitivity of all NMR experiments therefore strongly depends on the ability to recover rapidly the initial polarization state after its use in the previous transient. Whereas in "standard" liquid- and solid-state NMR experiments the return to equilibrium of nuclear polarization is induced by the incoherent fluctuation of surrounding magnetic interactions and is dictated by the longitudinal spin-lattice relaxation time constant $T_{1n}$, in experiments using hyperpolarization it will be dominated by the time required to create the hyperpolarized state.

[d] The same behavior would be expected for BDPA-TEMPO biradicals.[68]

Indeed, the best biradical we can imagine, with the highest $\varepsilon_B$, will be quite inefficient in terms of sensitivity if the time required to build the hyperpolarized nuclear spin state with this PA is very long. As seen previously, under conditions of MAS-CE, the build-up time constant for nuclear hyperpolarization, $T_B$, depends particularly on the efficiency of the individual rotor events to polarize the coupled nuclear spins and of spin diffusion to transfer this polarization to all further homonuclei in the sample.[e] Due to the complexity of the CE process in a spin-system large enough to account correctly for homonuclear spin–diffusion as well, the exact $T_B$ is very difficult to predict with simulations, although satisfactory trends can still be obtained (see Figure 6).[33] In contrast, it can easily be measured with a saturation-recovery experiment. It is interesting and important to note that as the mechanism leading to the depolarized nuclear spin state in absence of μwaves is exactly the same as for hyperpolarization, namely CE and homonuclear spin-diffusion, the same build-up time (or apparent $T_1$) is observed in the "off" as in the "on" experiment (for homogeneously distributed PAs).

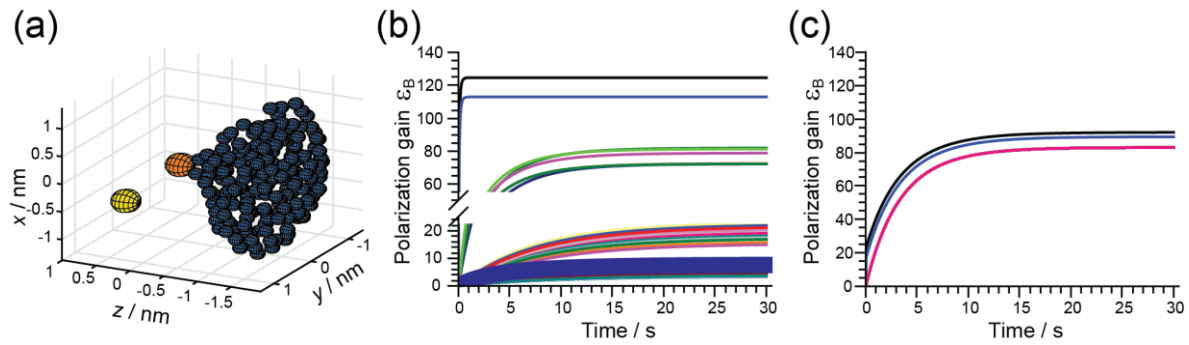


***Figure 6.*** *(a) Example of the spin system used in the bulk model at the base of simulations in (b) and (c). The orange and yellow spheres correspond to electron 1 and 2, and the blue spheres to 182 nuclear spins. (b-c) Bulk model simulations of the polarization build-up $\varepsilon_B$ for the nuclear spins without (b), and with (c) nuclear-dipolar rotor events (i.e. nuclear spin-diffusion). The black curve corresponds to the first proton (the one closest to the electrons), the blue curve to the second proton, and all other colored curves to further protons. In (b), the thick blue curve represents the mean nuclear polarization build-up. In (c), the pink curve represents the common polarization build-up of the further protons.*

[e] It is therefore based among others on coherent interactions and in this sense cannot be considered as relaxation induced by incoherent averaging. Note that paramagnetic-induced relaxation can affect $T_{1n}$ of surrounding nuclei and as such only indirectly impact the level of hyperpolarization $\varepsilon_B$ and the buildup time $T_B$.[33]

*Simulations were performed using the TOTAPOL geometry with $\omega_{1e}/2\pi$ = 0.85 MHz, $T_{1e}$ = 0.3 ms, $T_{2e}$ =1 ms, hyperfine coupling = 3 MHz, $\omega_{mw}/2\pi$ =263.45 GHz, $B_0$ = 9.394 T, and $\nu_r$ = 8 kHz. The bulk relaxation time of the nuclear spins was $T_{1n,Bulk}$ = 10 s, the closest proton relaxation time was $T_{1,n1}$ = 0.15 s. Adapted from Ref. [*33*] with permission from the PCCP Owner Societies.*

The hyperpolarization performance of a radical is thus entirely (and therefore best) characterized by both the real enhancement ratio with respect to Boltzmann equilibrium, $\varepsilon_B$, which should be as high as possible, and the build-up time constant $T_B$, which needs to be as short as possible. For best comparison, they can be combined in the expression $\varepsilon_B/\sqrt{T_B}$, which respects their relative weight towards experimental sensitivity. As an example, Fig. 5b compares the performances for 4 different water-soluble biradicals. Whereas the $\varepsilon_B$ values are quite similar for AMUPol, TEMTriPol-1 and AsymPolPOK, the efficiency of AsymPolPOK expressed as $\varepsilon_B/\sqrt{T_B}$ is much higher thanks to its very short relative build-up time constant.

It should be noted that the performance of PAs has also been expressed using the "practical sensitivity gain", $E = \varepsilon_{\text{abs}} \cdot \sqrt{T_{1n,\text{undoped}}/T_B}$ ,[34,37] with $\varepsilon_{\text{abs}}$ being the absolute enhancement ratio, which takes into account depolarization and quenching effects due to the presence of paramagnetic species inside the sample, and $T_{1\text{n,undoped}}$, the nuclear longitudinal relaxation time constant measured under identical conditions but without radicals inside the sample. In addition, first to be more complicated to determine and second to exaggerate practical sensitivity gains due to usually large $T_{1\text{n,undoped}}$ at the cryogenic temperatures still required for DNP, it introduces additional factors that do not depend on the nature of the radical itself, but more on its presence (quenching) and on the quality of the glassy state of the sample ($T_{1\text{n,undoped}}$). Moreover, misconceptions will arise when comparing biradicals dissolved in different solvents with dissimilar $T_{1\text{n,undoped}}$. We recommend therefore to use $\varepsilon_B/\sqrt{T_B}$ for the characterization of PAs. Other factors impacting the overall DNP sensitivity will be treated in the next section.

## 3. What else should we consider?

Whereas the nature of the radical will have a direct impact on the sensitivity of the DNP experiment through its efficiency in hyperpolarizing, expressed by the parameters $\varepsilon_B$ and $T_B$, many other factors play a role in the absolute sensitivity of a DNP-enhanced NMR spectrum, defined as the signal-to-noise ratio per the square-root of the experimental time, $(S/N)_{\sqrt{t}}$. All these factors are linked to the particular physical and chemical experimental conditions used to perform DNP experiments. It is important to keep these factors in mind, as the best DNP enhancement can be counterbalanced by unfavorable conditions, such that a study using standard solid-state NMR without DNP may be finally more appropriate.[38] The main experimental factors which strongly impact the sensitivity of DNP experiments are reviewed here.

**The temperature.** DNP experiments are standardly performed at temperatures around 100 K. Lowering the temperature produces a gain in sensitivity which is threefold: an increase of magnetization (Boltzmann distribution), a decrease of the thermal noise due to the cooling of some of the detection devices, and an improved efficiency of the CE DNP mechanism thanks to the slowdown of the spins' relaxation (see Fig. 7a). However, temperature can have an indirect effect on the spectral linewidths as well, in particular for systems that can present fast and large amplitude motions. Indeed, whereas dynamics at higher temperatures may help to obtain narrow resonances by averaging out structural heterogeneity, decrease of the temperature below the glass transition will freeze the system in a distribution of conformations characterized by inhomogeneously-broadened resonances of lower intensity. The opposite effect may occur with an increase in sensitivity at lower temperature for highly flexible sites that are difficult to

observe at room temperature. Sample temperature has also an effect on all other spin lifetimes, e.g. $T_B$, $T_{1\rho}$, or $T_2$', as can be seen in Figure 7a. This will be commented further below.

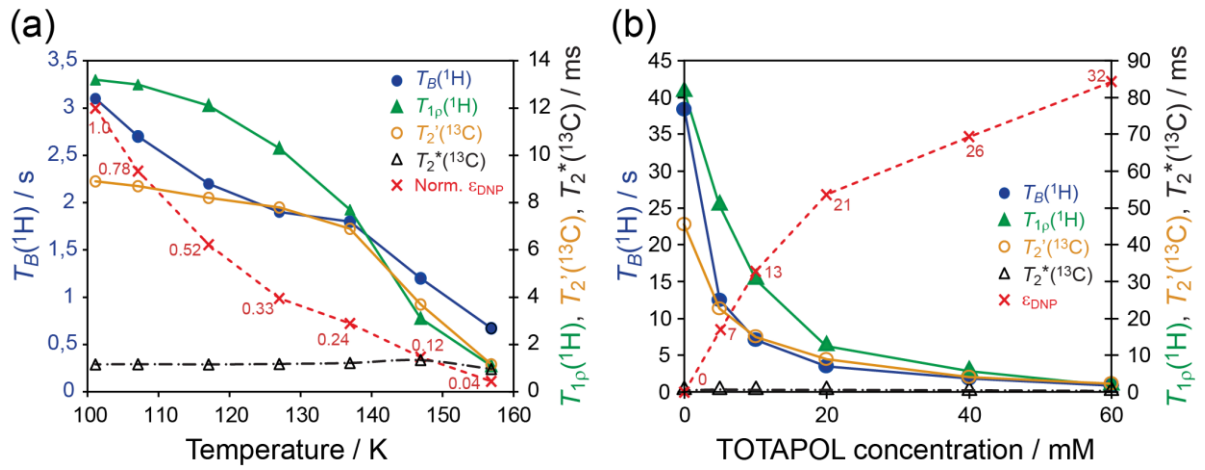


***Figure 7.*** *Temperature (a) and TOTAPOL concentration (b) dependence of DNP enhancement* $\varepsilon_{on/off}$ *(red crosses) and different lifetimes (*$T_B$ *in blue full circles,* $T_{1\rho}$ *in green full triangles,* $T_2$*' in orange open circles,* $T_2$** in black open triangles) on 2 M* $^{13}$*C-urea in* $d_6$*-DMSO/*$D_2O$*/*$H_2O$ *(6:3:1 by volume) at 9.4 T. For (a), the TOTAPOL concentration was 20 mM TOTAPOL. For (b), the temperature was 105 K. Adapted from Ref. [39] with permission from Elsevier.*

**The effective (or detectable) sample amount.** In solid-state MAS NMR, the sample is usually in the form of a powder which is directly inserted inside the MAS rotor. The limitation in detectable sample originates solely from the rotor volume, chosen as a function of the available probes, the desired MAS frequency, and the sample availability. For DNP, several aspects have to be considered. First, the presence of paramagnetic PAs inside the sample broadens and potentially shifts the resonances of the closest neighboring nuclear spins beyond detection. Part of the sample becomes invisible (bleaching/quenching effect), reducing thus the effective amount of sample which gives rise to signal. The amount of bleaching depends on the radical concentration,[37,40–42] the type of PA and of the directly hyperpolarized nuclear spin. Second, the polarizing agent is best uniformly distributed inside the sample. This can require specific sample preparation techniques, which may result in a dilution of the sample in the fixed volume of the rotor, compared to standard solid-state NMR. The original sample preparation consisting in the use of a glassy frozen solution[6] is quite inefficient in terms of effective

detectable number of spins and sensitivity. It is still used for the evaluation of PA performances or DNP mechanism investigations, but for applications other methods that minimize the dilution of the sample, such as impregnation,[43] film casting,[44] or matrix-free protocols,[26,45,46] have been developed and are preferred. It is to note that removal of the solvent in the matrix-free approach may be deleterious for the DNP enhancement through aggregation or phase separation of the hyperpolarizing agent. This can be avoided by the use of a direct or indirect affinity of the PA with the analyte.[26,45,37] In particular, chemical grafting of DNP radicals on the system of interest itself or its specific ligand has been proposed in biomolecular applications to target the signal enhancement.[47–55]

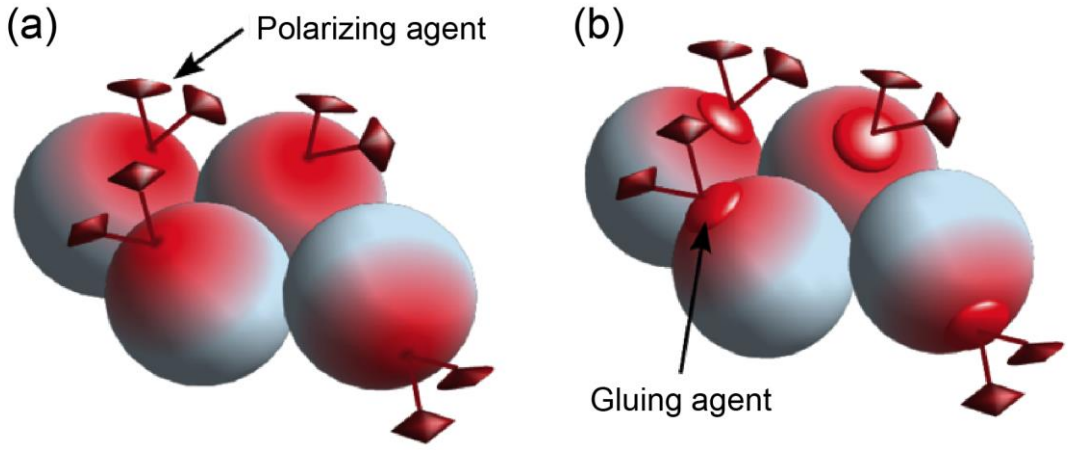


***Figure 8.*** *Schematic illustration of the two matrix-free preparation strategies using either a direct (a) or an indirect (b) affinity of PAs to the system of interest. Targeted DNP obtained by grafting the PA directly onto the system or to a ligand of the system can be seen as special cases of (a) or (b). Adapted with Ref. [45] with permission from The Royal Society of Chemistry.*

**The coherence lifetimes.** The sensitivity of an experiment depends on the type of experiment, and more specifically on the lifetime of the coherences present during the course of the pulse sequence, e.g. during mixing times, echoes, *J*-evolution periods, acquisition (see Figure 9b), etc. The temperature, as well as the amount of paramagnetic polarizing agent used for DNP have a strong effect on all coherence lifetimes, as can be seen in Figure 7.[39] This effect has to be properly investigated in order to choose the optimal PA concentration, which may be

different for one type of experiment to the other. For instance, 20 mM TOTAPOL reduces $^{13C}T_2$' from 45 to 10 ms for $^{13}$C-urea in DMSO/water (see Figure 7b). This would reduce the efficiency of a *J*-based homonuclear correlation experiment such as refocused INADEQUATE[56] or SARCOSY[57] by approximately a factor of 2.

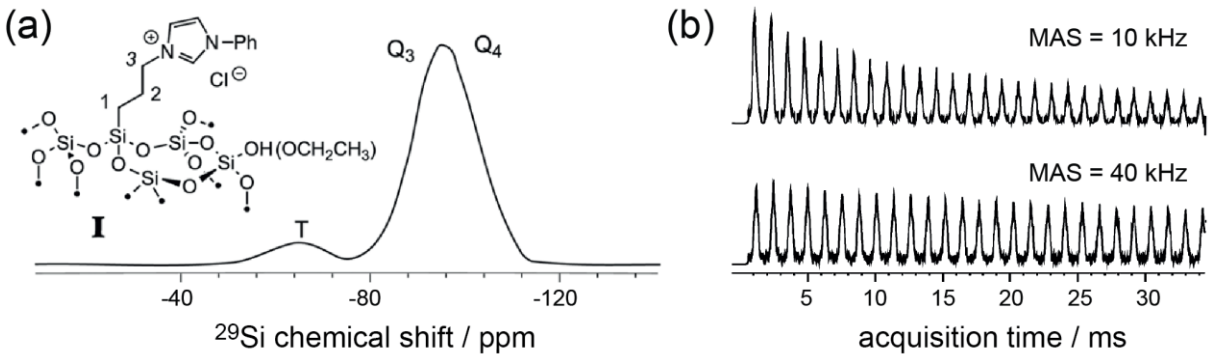


***Figure 9.*** *(a) DNP-enhanced {$^1$H-}$^{29}$Si CPMAS NMR spectrum of* ***I*** *impregnated with 10 mM AMUPol in 90:10 $D_2O/H_2O$, recorded at 18.8 T and ~115 K, using a MAS rate of 40 kHz and CPMG acquisition (summation of 60 whole echoes). (b) Free induction decays of experiment from (a) recorded at 10 and 40 kHz MAS rate. Adapted from Ref. [*58*] published by the PCCP Owner Societies.*

**Magnetic field, MAS frequency, rotor size, etc.** Even if the available magnetic fields and MAS probes for DNP are diversifying (see Figure 9), the range of possibilities are still much more reduced for DNP compared to conventional solid-state NMR. Notably, rotors of the same size, and therefore of the same theoretical capacity in terms of sample amount, can achieve only reduced MAS frequencies at 100 K due to the change in density of nitrogen gas.[f] As known from standard NMR, all these instrumental aspects do impact on the sensitivity and resolution of NMR experiments.

The fact that the sensitivity of the DNP experiment is affected by many other experimental parameters in addition to the DNP enhancement has been addressed by various groups, and different ways of correcting $\varepsilon_{on/off}$ (or $\varepsilon_B$) have been proposed to take into account

[f] A solution to that problem is to use helium gas instead, which however requires recovery of the turbine driving and cooling gas through a closed-loop system to be sustainable.[19,20]

some of these parameters. Thus, a quenching factor and the square-root of the ratio of longitudinal build-up times have been introduced by Rossini *et al.*[40], for example, to obtain a global enhancement factor. Similarly, the "practical sensitivity gain", $E = \varepsilon_{\text{abs}} \cdot \sqrt{T_{1n,\text{undoped}}/T_B}$,[34,37] takes also into account the change in apparent recovery time and the bleaching effect. The impact of the presence of solvent, the change in temperature and in some coherence lifetimes has been additionally considered by Kobayashi *et al.* in their global sensitivity enhancement.[59]

Correct identification and estimation of these various contributions for a proper correction of $\varepsilon_{\text{on/off}}$ is important to further develop DNP, but is very time consuming and impossible to envisage for each application. This is the reason we introduced in 2012 the absolute sensitivity ratio, ASR, which expresses the measured experimental sensitivity gain brought by DNP.[26,38] Instead of correcting $\varepsilon_{\text{on/off}}$ for the separate contributions affecting sensitivity, the empirical ASR is obtained by comparing the S/N per unit square root of time from a spectrum obtained under optimal DNP conditions with one obtained under optimal standard NMR conditions. The advantage of the ASR is that it intrinsically takes into account all possible experimental contributions that may impact on the sensitivity of the DNP experiment compared to a reference solid-state NMR experiment, including potential differences in available equipment (magnetic field, type of probe, etc.), with the acquisition of only two 1D spectra. Depending on the study, the standard NMR reference spectrum may be taken under conditions which are in part similar to the DNP spectrum, such as at low temperature, leading to a so called *reduced ASR*. The disadvantage of the ASR is that sometimes DNP is so effective that a conventional reference spectrum is impossible to acquire.[60,61] The same limitation is obviously present for $\varepsilon_{\text{on/off}}$, $\varepsilon_{\text{B}}$, $E$, etc.

## 4. Conclusions

Realizing that the goal of MAS-DNP is generally to increase the sensitivity of NMR experiments to address systems and questions that were beyond reach, e.g. detection and correlation of low-gamma and/or low isotopic abundance spins, a proper characterization of the sensitivity increase is therefore essential. In the jungle of factors and ratios, DNP enhancement, depolarization, quenching, bleaching, global enhancement, practical, global, overall or absolute sensitivity, it may be difficult to choose the correct way of doing it. This task is even more difficult considering that all these factors actually contain some information, but none of them is the perfect candidate to choose in any particular case. In addition, some of them are much easier to obtain than others, and we may be tempted to favor those even if the information content is not the most appropriate. The chosen factor should reflect the correct information content and therefore match the type of investigation.

The DNP enhancement factor $\varepsilon_{on/off}$, the easiest one to measure, does not give by itself any information about the sensitivity of the experiment. However, it is a good indication to evaluate whether the DNP process is working in a particular sample. Indeed, the DNP efficiency relies very much on the quality of the DNP sample preparation in terms e.g. of glass properties, concentration and distribution of the hyperpolarizing agent. Progress in sample preparation can easily be followed by $\varepsilon_{on/off}$.

Investigating the efficiency of a polarizing agent, or of different DNP mechanisms, is at the heart of many studies aiming at improving the DNP technique itself in order to broaden its applicability to any kind of systems and conditions (higher magnetic fields, higher or lower temperatures, faster spinning, etc.). In such cases, it is important to take into account the efficiency in both the enhancement and the build-up time. A particular attention has to be paid to potential depolarization effects whose importance is dependent on the radical, the DNP

mechanism and the experimental conditions. For such studies, it should be absolutely mandatory to report both the Boltzmann enhancement $\varepsilon_B$ and the DNP build-up time $T_B$.

For applications, the ASR is very convenient to highlight the pertinence of using DNP-enhanced NMR for experiments that would be very time consuming under standard NMR conditions. It nicely underlines the broadened range of experimental possibilities that are offered by MAS-DNP for the structural investigation of various systems. For example, in the case of functionalized silica nanoparticles, an ASR value of 25 has been reported for the DNP-enhanced $^{29}$Si CPMAS experiment, corresponding to an experimental time saving factor of 625 ($ASR^2$).[62] This huge gain in sensitivity allowed the acquisition of $^{29}$Si-$^{29}$Si correlation experiment within a few hours, despite the low natural abundance (NA) of $^{29}$Si (4.7 %). This experiment, which would have been impossible without DNP, was key to understanding the type of organosiloxane polymerization at the surface of the nanoparticles. $^{13}$C-$^{13}$C and $^{15}$N-$^{13}$C correlations at NA are also extremely challenging considering the isotopic abundance of 1.1% for $^{13}$C and 0.4 % for $^{15}$N. A $^{13}$C-$^{13}$C correlation experiment on cellulose at NA was shown to be possible with DNP in only 20 minutes instead of several days thanks to an ASR of 47 (timesaving of more than 2000),[26] and the first $^{15}$N-$^{13}$C correlation at NA was demonstrated on a guanosine derivative within 25 h (ASR of more than 10).[63]

MAS-DNP has slowly reached a regime where new methodology can be developed such that it can be used to answer important structural questions. In such cases, the only relevant question is whether the sensitivity of a particular sample is high enough to envisage the use of a certain methodology, without worrying about where the sensitivity is coming from (DNP, temperature, short build-up times, etc.). This requires that authors of new methodologies developed at the limit of the NMR sensitivity take the habit to give an indication of the signal-to-noise ratio per square root of the experimental time $(S/N)/\sqrt{t_{exp}}$ for the system used to

demonstrate their methodology. This has not been done so far, but would definitively help scientists to decide on the best strategy to unravel structural information from their system using NMR, including DNP-enhanced NMR. Thus, having access to the original data from the few examples given above, we obtained values for $(S/N)_{\sqrt{t}}$ of 20 $s^{-1/2}$ for the $\{^{1}H\text{-}\}^{29}Si$ CPMAS spectrum measured on the nanoparticle sample used for the $^{29}Si$-$^{29}Si$ correlation experiments of Ref. [62], 130 $s^{-1/2}$ for the $\{^{1}H\text{-}\}^{13}C$ CPMAS spectrum of the cellulose sample which allowed the acquisition of a $^{13}C$-$^{13}C$ correlation experiment in 20 min,[26] 15 $s^{-1/2}$ for the $\{^{1}H\text{-}\}^{13}C$ CPMAS spectrum of the guanosine sample on which the $^{15}N$-$^{13}C$ correlation experiment at NA was demonstrated.[63] As a further example, the measurement of $^{13}C$-$^{13}C$ distances at NA that allowed to predict the crystal structure of cyclo-FF nanotubes[64,65] relied on a $(S/N)_{\sqrt{t}}$ value of 80 $s^{-1/2}$ (measured on the $\{^{1}H\text{-}\}^{13}C$ CPMAS spectrum).

Even if MAS-DNP has now developed so far that it can be considered as a complementary powerful tool for the structural investigation of a multitude of interesting and complex systems, there is still much room for further improvements of the technique itself. Instrumentation, methodology and application will all continue to evolve in parallel and the description of their various impacts on the NMR sensitivity will still need to be best described using the appropriate factor. We hope that this overview on DNP enhancements for solid-state NMR has given a good indication of how best to proceed with this in mind.

## Acknowledgments

This work was supported by the French National Research Agency (ANR-16-C81L-0030-03, ANR-12-BS08-0016-01, ANR-11-LABX-0003-01 and RTB) and the European Research Council (ERC-CoG- 2015, No. 682895). The National High Magnetic Field

Laboratory is supported by National Science Foundation through NSF/DMR-1644779 and the State of Florida.

## References


1. T. R. Carver and C. P. Slichter. Polarization of Nuclear Spins in Metals. *Phys. Rev.* **92,** 212–213 (1953).

2. V. S. Bajaj, C. T. Farrar, M. K. Hornstein, I. Mastovsky, J. Vieregg, J. Bryant, B. Eléna, K. E. Kreischer, R. J. Temkin and R. G. Griffin. Dynamic nuclear polarization at 9 T using a novel 250 GHz gyrotron microwave source. *J. Magn. Reson.* **160,** 85–90 (2003).

3. T. Maly, G. T. Debelouchina, V. S. Bajaj, K.-N. Hu, C.-G. Joo, M. L. Mak–Jurkauskas, J. R. Sirigiri, P. C. A. van der Wel, J. Herzfeld, R. J. Temkin, *et al.* Dynamic nuclear polarization at high magnetic fields. *J. Chem. Phys.* **128,** 52211 (2008).

4. R. G. Griffin and T. F. Prisner. High field dynamic nuclear polarization—the renaissance. *Phys. Chem. Chem. Phys.* **12,** 5737–5740 (2010).

5. L. R. Becerra, G. J. Gerfen, R. J. Temkin, D. J. Singel and R. G. Griffin. Dynamic nuclear polarization with a cyclotron resonance maser at 5 T. *Phys. Rev. Lett.* **71,** 3561–3564 (1993).

6. G. J. Gerfen, L. R. Becerra, D. A. Hall, R. G. Griffin, R. J. Temkin and D. J. Singel. High frequency (140 GHz) dynamic nuclear polarization: Polarization transfer to a solute in frozen aqueous solution. *J. Chem. Phys.* **102,** 9494–9497 (1995).

7. K.-N. Hu, H. Yu, T. M. Swager and R. G. Griffin. Dynamic Nuclear Polarization with Biradicals. *J. Am. Chem. Soc.* **126,** 10844–10845 (2004).

8. C. Song, K. Hu, C. Joo, T. M. Swager and R. G. Griffin. TOTAPOL: A Biradical Polarizing Agent for Dynamic Nuclear Polarization Experiments in Aqueous Media. *J. Am. Chem. Soc.* **128,** 11385–11390 (2006).

9. M. Rosay, L. Tometich, S. Pawsey, R. Bader, R. Schauwecker, M. Blank, P. M. Borchard, S. R. Cauffman, K. L. Felch, R. T. Weber, *et al.* Solid-state dynamic nuclear polarization at 263 GHz: spectrometer design and experimental results. *Phys. Chem. Chem. Phys.* **12,** 5850–5860 (2010).

10. Y. Matsuki, T. Maly, O. Ouari, H. Karoui, F. Le Moigne, E. Rizzato, S. Lyubenova, J. Herzfeld, T. Prisner, P. Tordo, *et al.* Dynamic Nuclear Polarization with a Rigid Biradical. *Angew. Chemie Int. Ed.* **48,** 4996–5000 (2009).

11. E. L. Dane, B. Corzilius, E. Rizzato, P. Stocker, T. Maly, A. A. Smith, R. G. Griffin, O. Ouari, P. Tordo and T. M. Swager. Rigid orthogonal bis-TEMPO biradicals with improved solubility for dynamic nuclear polarization. *J. Org. Chem.* **77,** 1789–1797 (2012).

12. M. K. Kiesewetter, B. Corzilius, A. A. Smith, R. G. Griffin and T. M. Swager. Dynamic Nuclear Polarization with a Water-Soluble Rigid Biradical. *J. Am. Chem. Soc.* **134,** 4537–4540 (2012).

13. A. Zagdoun, G. Casano, O. Ouari, G. Lapadula, A. J. Rossini, M. Lelli, M. Baffert, D. Gajan, L. Veyre, W. E. Maas, *et al.* A slowly relaxing rigid biradical for efficient dynamic nuclear polarization surface-enhanced NMR spectroscopy: Expeditious

characterization of functional group manipulation in hybrid materials. *J. Am. Chem. Soc.* **134,** 2284–2291 (2012).

14. A. Zagdoun, G. Casano, O. Ouari, M. Schwarzwälder, A. J. Rossini, F. Aussenac, M. Yulikov, G. Jeschke, C. Copéret, A. Lesage, *et al.* Large Molecular Weight Nitroxide Biradicals Providing Efficient Dynamic Nuclear Polarization at Temperatures up to 200 K. *J. Am. Chem. Soc.* **135,** 12790–12797 (2013).

15. C. Sauvée, M. Rosay, G. Casano, F. Aussenac, R. T. Weber, O. Ouari and P. Tordo. Highly Efficient, Water-Soluble Polarizing Agents for Dynamic Nuclear Polarization at High Frequency. *Angew. Chemie Int. Ed.* **52,** 10858–10861 (2013).

16. D. J. Kubicki, G. Casano, M. Schwarzwälder, S. Abel, C. Sauvée, K. Ganesan, M. Yulikov, A. J. Rossini, G. Jeschke, C. Copéret, *et al.* Rational design of dinitroxide biradicals for efficient cross-effect dynamic nuclear polarization. *Chem. Sci.* **7,** 550–558 (2016).

17. C. Sauvée, G. Casano, S. Abel, A. Rockenbauer, D. Akhmetzyanov, H. Karoui, D. Siri, F. Aussenac, W. Maas, R. T. Weber, *et al.* Tailoring of Polarizing Agents in the bTurea Series for Cross-Effect Dynamic Nuclear Polarization in Aqueous Media. *Chem. - A Eur. J.* **22,** 5598–5606 (2016).

18. D. J. Kubicki, A. J. Rossini, A. Purea, A. Zagdoun, O. Ouari, P. Tordo, F. Engelke, A. Lesage and L. Emsley. Amplifying dynamic nuclear polarization of frozen solutions by incorporating dielectric particles. *J. Am. Chem. Soc.* **136,** 15711–15718 (2014).

19. E. Bouleau, P. Saint-Bonnet, F. Mentink-Vigier, H. Takahashi, J.-F. Jacquot, M. Bardet, F. Aussenac, A. Purea, F. Engelke, S. Hediger, *et al.* Pushing NMR sensitivity limits using dynamic nuclear polarization with closed-loop cryogenic helium sample spinning. *Chem. Sci.* **6,** 6806–6812 (2015).

20. D. Lee, E. Bouleau, P. Saint-Bonnet, S. Hediger and G. De Paëpe. Ultra-low temperature MAS-DNP. *J. Magn. Reson.* **264,** 116–124 (2016).

21. K. R. Thurber and R. Tycko. Theory for cross effect dynamic nuclear polarization under magic-angle spinning in solid state nuclear magnetic resonance: The importance of level crossings. *J. Chem. Phys.* **137,** 84508 (2012).

22. F. Mentink-Vigier, U. Akbey, Y. Hovav, S. Vega, H. Oschkinat and A. Feintuch. Fast passage dynamic nuclear polarization on rotating solids. *J. Magn. Reson.* **224,** 13–21 (2012).

23. F. Mentink-Vigier, Ü. Akbey, H. Oschkinat, S. Vega and A. Feintuch. Theoretical aspects of Magic Angle Spinning - Dynamic Nuclear Polarization. *J. Magn. Reson.* **258,** 102–120 (2015).

24. E. A. Nanni, A. B. Barnes, Y. Matsuki, P. P. Woskov, B. Corzilius, R. G. Griffin and R. J. Temkin. Microwave field distribution in a magic angle spinning dynamic nuclear polarization NMR probe. *J. Magn. Reson.* **210,** 16–23 (2011).

25. E. P. Saliba, E. L. Sesti, F. J. Scott, B. J. Albert, E. J. Choi, N. Alaniva, C. Gao and A. B. Barnes. Electron Decoupling with Dynamic Nuclear Polarization in Rotating Solids. *J. Am. Chem. Soc.* **139,** 6310–6313 (2017).

26. H. Takahashi, D. Lee, L. Dubois, M. Bardet, S. Hediger and G. De Paëpe. Rapid Natural-Abundance 2D 13C-13C Correlation Spectroscopy Using Dynamic Nuclear Polarization Enhanced Solid-State NMR and Matrix-Free Sample Preparation. *Angew. Chemie Int. Ed.* **51,** 11766–11769 (2012).

27. Y. Hovav, O. Levinkron, A. Feintuch and S. Vega. Theoretical Aspects of Dynamic Nuclear Polarization in the Solid State: The Influence of High Radical Concentrations on the Solid Effect and Cross Effect Mechanisms. *Appl. Magn. Reson.* **43,** 21–41 (2012).

28. K. R. Thurber and R. Tycko. Perturbation of nuclear spin polarizations in solid state NMR of nitroxide-doped samples by magic-angle spinning without microwaves. *J. Chem. Phys.* **140,** 184201 (2014).

29. F. Mentink-Vigier, S. Paul, D. Lee, A. Feintuch, S. Hediger, S. Vega and G. De Paëpe. Nuclear depolarization and absolute sensitivity in magic-angle spinning cross effect dynamic nuclear polarization. *Phys. Chem. Chem. Phys.* **17,** 21824–21836 (2015).

30. A. S. Lilly Thankamony, J. J. Wittmann, M. Kaushik and B. Corzilius. Dynamic nuclear polarization for sensitivity enhancement in modern solid-state NMR. *Prog. Nucl. Magn. Reson. Spectrosc.* **102–103,** 120–195 (2017).

31. Y. Hovav, A. Feintuch and S. Vega. Theoretical aspects of dynamic nuclear polarization in the solid state - The cross effect. *J. Magn. Reson.* **214,** 29–41 (2012).

32. D. Wišniewski, A. Karabanov, I. Lesanovsky and W. Köckenberger. Solid effect DNP polarization dynamics in a system of many spins. *J. Magn. Reson.* **264,** 30–38 (2016).

33. F. Mentink-Vigier, S. Vega and G. De Paëpe. Fast and accurate MAS–DNP simulations of large spin ensembles. *Phys. Chem. Chem. Phys.* **19,** 3506–3522 (2017).

34. F. Mentink-Vigier, G. Mathies, Y. Liu, A.-L. Barra, M. A. Caporini, D. Lee, S. Hediger, R. G. Griffin and G. De Paëpe. Efficient cross-effect dynamic nuclear polarization without depolarization in high-resolution MAS NMR. *Chem. Sci.* **8,** 8150–8163 (2017).

35. F. Mentink-Vigier, I. Marin-Montesinos, A. P. Jagtap, J. Van Tol, S. Hediger, D. Lee, S. T. Sigurdsson and G. De Paëpe. AsymPol: a simple asymmetric bis-nitroxide for efficient dynamic nuclear polarization. *J. Am. Chem. Soc.* submitted

36. G. Mathies, M. A. Caporini, V. K. Michaelis, Y. Liu, K.-N. Hu, D. Mance, J. L. Zweier, M. Rosay, M. Baldus and R. G. Griffin. Efficient Dynamic Nuclear Polarization at 800 MHz/527 GHz with Trityl-Nitroxide Biradicals. *Angew. Chemie* **127,** 11936–11940 (2015).

37. B. Corzilius, L. B. Andreas, A. A. Smith, Q. Z. Ni and R. G. Griffin. Paramagnet induced signal quenching in MAS–DNP experiments in frozen homogeneous solutions. *J. Magn. Reson.* **240,** 113–123 (2014).

38. D. Lee, S. Hediger and G. De Paëpe. Is solid-state NMR enhanced by dynamic nuclear polarization? *Solid State Nucl. Magn. Reson.* **66–67,** 6–20 (2015).

39. H. Takahashi, C. Fernández-de-Alba, D. Lee, V. Maurel, S. Gambarelli, M. Bardet, S. Hediger, A.-L. A.-L. Barra and G. De Paëpe. Optimization of an absolute sensitivity in a glassy matrix during DNP-enhanced multidimensional solid-state NMR experiments. *J. Magn. Reson.* **239,** 91–99 (2014).

40. A. J. Rossini, A. Zagdoun, M. Lelli, D. Gajan, F. Rascón, M. Rosay, W. E. Maas, C. Copéret, A. Lesage and L. Emsley. One hundred fold overall sensitivity enhancements for Silicon-29 NMR spectroscopy of surfaces by dynamic nuclear polarization with CPMG acquisition. *Chem. Sci.* **3,** 108–115 (2012).

41. S. Lange, A. H. Linden, Ü. Akbey, W. Trent Franks, N. M. Loening, B.-J. van Rossum and H. Oschkinat. The effect of biradical concentration on the performance of DNP-MAS-NMR. *J. Magn. Reson.* **216,** 209–212 (2012).

42. R. Rogawski, I. V. Sergeyev, Y. Zhang, T. H. Tran, Y. Li, L. Tong and A. E. McDermott. NMR Signal Quenching from Bound Biradical Affinity Reagents in DNP Samples. *J. Phys. Chem. B* **121,** 10770–10781 (2017).

43. A. Lesage, M. Lelli, D. Gajan, M. A. Caporini, V. Vitzthum, P. Mieville, J. Alauzun, A. Roussey, C. Thieuleux, A. Mehdi, *et al.* Surface Enhanced NMR Spectroscopy by Dynamic Nuclear Polarization. *J. Am. Chem. Soc.* **132,** 15459–15461 (2010).

44. D. Le, G. Casano, T. Phan, F. Ziarelli, O. Ouari, F. Aussenac, P. Thureau, G. Mollica, D. Gigmes, P. Tordo, *et al.* Optimizing sample preparation methods for dynamic nuclear polarization solid-state NMR of synthetic polymers. *Macromolecules* **47,** 3909−3916 (2014).

45. H. Takahashi, S. Hediger and G. De Paëpe. Matrix-free dynamic nuclear polarization enables solid-state NMR 13C–13C correlation spectroscopy of proteins at natural isotopic abundance. *Chem. Commun.* **49,** 9479–9481 (2013).

46. C. Fernández-de-Alba, H. Takahashi, A. Richard, Y. Chenavier, L. Dubois, V. Maurel, D. Lee, S. Hediger and G. De Paëpe. Matrix-Free DNP-Enhanced NMR Spectroscopy of Liposomes Using a Lipid-Anchored Biradical. *Chem. - A Eur. J.* **21,** 4512–4517 (2015).

47. V. Vitzthum, F. Borcard, S. Jannin, M. Morin, P. Miéville, M. A. Caporini, A. Sienkiewicz, S. Gerber-Lemaire and G. Bodenhausen. Fractional spin-labeling of polymers for enhancing NMR sensitivity by solvent-free dynamic nuclear polarization. *ChemPhysChem* **12,** 2929–2932 (2011).

48. T. Maly, D. Cui, R. G. Griffin and A. F. Miller. 1H dynamic nuclear polarization based on an endogenous radical. *J. Phys. Chem. B* **116,** 7055–7065 (2012).

49. A. N. Smith, M. A. Caporini, G. E. Fanucci and J. R. Long. A Method for Dynamic Nuclear Polarization Enhancement of Membrane Proteins. *Angew. Chemie Int. Ed.* **54,** 1542–1546 (2015).

50. M. Kaushik, T. Bahrenberg, T. V. Can, M. A. Caporini, R. Silvers, J. Heiliger, A. A. Smith, H. Schwalbe, R. G. Griffin and B. Corzilius. Gd(III) and Mn(II) complexes for dynamic nuclear polarization: small molecular chelate polarizing agents and applications with site-directed spin labeling of proteins. *Phys. Chem. Chem. Phys.* **18,** 27205–27218 (2016).

51. M. A. Voinov, D. B. Good, M. E. Ward, S. Milikisiyants, A. Marek, M. A. Caporini, M. Rosay, R. A. Munro, M. Ljumovic, L. S. Brown, *et al.* Cysteine-Specific Labeling of Proteins with a Nitroxide Biradical for Dynamic Nuclear Polarization NMR. *J. Phys. Chem. B* **119,** 10180–10190 (2015).

52. E. A. W. van der Cruijsen, E. J. Koers, C. Sauvée, R. E. Hulse, M. Weingarth, O. Ouari, E. Perozo, P. Tordo and M. Baldus. Biomolecular DNP-Supported NMR Spectroscopy using Site-Directed Spin Labeling. *Chem. - A Eur. J.* **21,** 12971–12977 (2015).

53. B. J. Wylie, B. G. Dzikovski, S. Pawsey, M. Caporini, M. Rosay, J. H. Freed and A. E. McDermott. Dynamic nuclear polarization of membrane proteins: covalently bound spin-labels at protein–protein interfaces. *J. Biomol. NMR* **61,** 361–367 (2015).

54. T. Viennet, A. Viegas, A. Kuepper, S. Arens, V. Gelev, O. Petrov, T. N. Grossmann, H. Heise and M. Etzkorn. Selective Protein Hyperpolarization in Cell Lysates Using Targeted Dynamic Nuclear Polarization. *Angew. Chemie Int. Ed.* **55,** 10746–10750 (2016).

55. R. Rogawski and A. E. McDermott. New NMR tools for protein structure and function: Spin tags for dynamic nuclear polarization solid state NMR. *Arch. Biochem. Biophys.* **628,** 102–113 (2017).

56. A. Lesage, M. Bardet and L. Emsley. Through-Bond Carbon−Carbon Connectivities in Disordered Solids by NMR. *J. Am. Chem. Soc.* **121,** 10987–10993 (1999).

57. D. Lee, J. Struppe, D. W. Elliott, L. J. Mueller and J. J. Titman. Sensitive absorptive refocused scalar correlation NMR spectroscopy in solids. *Phys. Chem. Chem. Phys.* **11,** 3547–3553 (2009).

58. S. R. Chaudhari, P. Berruyer, D. Gajan, C. Reiter, F. Engelke, D. L. Silverio, C. Copéret, M. Lelli, A. Lesage and L. Emsley. Dynamic nuclear polarization at 40 kHz magic angle spinning. *Phys. Chem. Chem. Phys.* **18,** 10616–10622 (2016).

59. T. Kobayashi, O. Lafon, A. S. Lilly Thankamony, I. I. Slowing, K. Kandel, D. Carnevale, V. Vitzthum, H. Vezin, J.-P. Amoureux, G. Bodenhausen, *et al.* Analysis of sensitivity enhancement by dynamic nuclear polarization in solid-state NMR: a case study of functionalized mesoporous materials. *Phys. Chem. Chem. Phys.* **15,** 5553–5562 (2013).

60. F. Blanc, L. Sperrin, D. Lee, R. Dervişoğlu, Y. Yamazaki, S. M. Haile, G. De Paëpe, C. P. Grey, R. Dervişoğlu, Y. Yamazaki, *et al.* Dynamic Nuclear Polarization NMR of Low-γ Nuclei: Structural Insights into Hydrated Yttrium-Doped BaZrO 3. *J. Phys. Chem. Lett.* **5,** 2431–2436 (2014).

61. D. Lee, C. Leroy, C. Crevant, L. Bonhomme-Coury, F. Babonneau, D. Laurencin, C. Bonhomme and G. De Paëpe. Interfacial Ca2+ environments in nanocrystalline apatites revealed by dynamic nuclear polarization enhanced 43Ca NMR spectroscopy. *Nat. Commun.* **8,** 14104 (2017).

62. D. Lee, G. Monin, N. T. Duong, I. Z. Lopez, M. Bardet, V. Mareau, L. Gonon and G. De Paëpe. Untangling the Condensation Network of Organosiloxanes on Nanoparticles using 2D 29 Si–29Si Solid-State NMR Enhanced by Dynamic Nuclear Polarization. *J. Am. Chem. Soc.* **136,** 13781–13788 (2014).

63. K. Märker, M. Pingret, J. M. Mouesca, D. Gasparutto, S. Hediger and G. De Paëpe. A New Tool for NMR Crystallography: Complete 13C/15N Assignment of Organic Molecules at Natural Isotopic Abundance Using DNP-Enhanced Solid-State NMR. *J. Am. Chem. Soc.* **137,** 13796–13799 (2015).

64. K. Märker, S. Paul, C. Fernández-de-Alba, D. Lee, J.-M. Mouesca, S. Hediger and G.

De Paëpe. Welcoming natural isotopic abundance in solid-state NMR: probing π-stacking and supramolecular structure of organic nanoassemblies using DNP. *Chem. Sci.* **8,** 974–987 (2017).

65. K. Märker, S. Paul, D. Lee, J.-M. Mouesca, S. Hediger and G. De Paëpe. NMR crystallography of organic molecules: Benefiting from natural isotopic abundance and MAS-DNP. in *10th Alpine Conference on Solid-State NMR* (2017).

66. A. Bornet and S. Jannin. Optimizing dissolution dynamic nuclear polarization. *J. Magn. Reson.* **264,** 13–21 (2016).

67. S. Un, T. Prisner, R. T. Weber, M. J. Seaman, K. W. Fishbein, A. E. McDermott, D. J. Singel, R. G. Griffin, S. Una, T. Prisnera, *et al.* Pulsed dynamic nuclear polarization at 5 T. *Chem. Phys. Lett.* **189,** 54–59 (1992).

68. E. L. Dane, T. Maly, G. T. Debelouchina, R. G. Griffin and T. M. Swager. Synthesis of a BDPA-TEMPO biradical. *Org. Lett.* **11,** 1871–1874 (2009).